IOP Conf. Series: Materials Science and Engineering **443** (2018) 012014 doi:10.1088/1757-899X/443/1/012014

Microstructure of luminescent $MgAl_2O_4$ nanoceramics

A N Kiryakov[1], A F Zatsepin[1], T V Dyachkova[2], A P Tytunyunnik[2], Yu G Zainulin[2], G Yakovlev[1], V A Pustovarov[1] and D R Bautimirov[1]

[1] Ural Federal University, 620002, Ekaterinburg, Russia
[2] Institute of Solid State Chemistry of the Ural Branch of the Russian Academy of Sciences, 620990, Ekaterinburg, Russia

arseny.kiriakov@urfu.ru

Abstract. Luminescent transparent nanoceramics were obtained by thermobaric treatment (TBT) of magnesium aluminium spinel nanopowder. The morphological features were studied by scanning electron microscopy combined with X-ray powder diffraction. Obtained ceramics do not have any agglomerates and pores larger than 100 nm. Crystallites have a high size uniformity. An increase in the lattice constant of nanoceramics compared to the initial powder is observed. Under the TBT, a decrease in the region of coherent scattering due to elastic deformation of crystallites is found. The absence of cracks, large pores, nanosize grains, and high size uniformity reduce light loss in the material, increasing its transparency. Point defects were characterized by photoluminescence and electron spin resonance (ESR) methods. The glow in the 1.8 eV band is caused by the presence of Ti^{3+} impurity ions. An abnormally wide peak with a maximum at 2.4 eV in the photoluminescence spectrum is recorded. This signal is a superposition of the Mn^{2+} ions emission bands and oxygen vacancies (F and F^+ centres). In the ESR spectrum, signals from impurity ions of iron, titanium, and manganese, as well as an intense signal at g = 2.005 associated with oxygen vacancies in nanoceramics were detected.

1. Introduction

Transparent ceramics with magnesium aluminium spinel (MAS) have promising applications in optoelectronics, photonics, and laser technology [1-3]. A wide light transmission window (0,2-5,5 μm), heat resistance, corrosion and radiation resistance, and high hardness allow such ceramics to compete with aluminium oxide, aluminium nitride, magnesium oxide, and zirconium oxide [4-6].

The transparency of the ceramic material depends on its morphology. First of all, the residual porosity, pore size, and grain size have a strong influence on transparency. According to Refs. [5,6], the main light losses in microceramics are caused by pores formed at the junction of several grain boundaries. The traditional approach of obtaining transparent ceramics including MAS is to reduce the residual porosity. It also implies a significant increase of grains, in order to minimize the reflection of transmitted light at their boundaries. To achieve optimal parameters of porosity and grain size, small amounts of special additives, such as LiF, which increase the mobility of interfaces and grains, are often used. Such microceramics have a crystallite size of 10 μm and higher. However, additives can adversely affect the physicochemical properties of spinel [5,6]. Preparation of the pure transparent ceramics of aluminium magnesium spinel is an important task, since it allows studying the material free from specially introduced impurities.

The pure transparent ceramics are sintered at high pressures and temperatures [7,8]. Interestingly, transparency in this case is achieved by maintaining nanograins with uniform size distribution. The pores

in such nanoceramics are replaced due to the fact that the particles of 30-50 nm size are subjected to plastic deformation, filling the entire free volume of the material without agglomerating. On the other hand, the formation of a large number of grain boundaries leads to an increase in the defectiveness of ceramics associated with dangling bonds [9]. The combination of scanning electron microscopy (SEM), photoluminescence (FL), and electron spin resonance (ESR) techniques allows for morphological analysis and determination of the nature of point defects in the material.

The aim of this work is to study the morphological, luminescent, and paramagnetic features of transparent nanoceramics of magnesium aluminium spinel.

2. Materials and methods

Nanopowder of magnesium aluminium spinel is obtained by precipitation from aluminium and magnesium nitrates with the addition of ammonia to control the pH of the system. The suspension was dried overnight at a temperature of 150°C. The gelling was carried out at 1000°C for 1 hour in air.

The resulting nanopowder was pressed into a cylindrical tablet 4×5 mm^2 in size and calcined in a vacuum oven for 3 hours at a temperature of 500°C to remove the sorbed impurities. The tablet was then placed in a standard pre-calibrated high-pressure chamber of the toroid type. The temperature was controlled by the power of the current passing through the graphite heater. To prevent carbon contamination, the inner walls of the graphite heater were insulated with platinum foil. The sample was compressed between the anvils of the press to the required pressure, and then the temperature was raised. After holding at the set temperature for 60 minutes, the sample under pressure was quenched by sudden dropping of temperature and pressure. Transparent nanoceramics of MAS were obtained at P = 4 GPa and T = 600°C.

The purity of synthesized product was checked using X-ray powder diffraction (XRD) patterns collected at room temperature on a STADI-P (Stoe) diffractometer equipped with a linear mini-PSD detector using $CuK\alpha^1$ radiation in the 2θ range 5° to 120° with a step of 0.02°. Polycrystalline silicon (a = 5.43075 (5) Å) was used as external standard. The PDF2 database of powder standards (ICDD, USA, Release 2016) was used to identify possible impurity phases. The unit cell parameters and mass fractions of $MgAl_2O_4$ were refined by Rietveld method using XRD data and the GSAS software [10,11].

The surface structure was studied using SIGMA VP scanning electron microscope (SEM, Carl Zeiss, Germany) and secondary electron detector (in-lens) in high vacuum at a 3 kV accelerating voltage. Registration of point defects in transparent nanoceramics of MAS is performed by photoluminescence measurements. The photoluminescence spectra measured at room temperature on a system equipped with a double prism monochromator type MDR-4, using a 400 W deuterium lamp and a photomultiplier R-6358-10 (Hamamatsu). Excitation spectra were corrected for the wavelength-dependent intensity variation using yellow lumogen with energy-independent quantum yield over the studied spectral range. Emission spectra are presented taking into account the correction for the spectral sensitivity of photomultiplier. An additional method of studying the heterogeneity of the crystal structure is to measure the electron spin resonance (ESR) spectra of the ceramics. The ESR signal was recorded at room temperature on a ELEXSYS 580 spectrometer (Bruker) with resonant frequency of 9.27 GHz. Photoluminescence and electron paramagnetic resonance (EPR) methods are applicable to the study of point defects, because they are sensitive to electrons weakly bound to an atom.

3. Results

3.1. X-ray powder diffraction

According to the results of XRD of the initial powder and transparent nanoceramics of MAS (Fig. 1), the samples have cubic symmetry ($Fd\bar{3}m$ space group). There is a small amount of MgO impurity phase (~3 mass%) both in the initial powder and in nanoceramics. TBT does not change the phase composition of ceramics. The size of the coherent scattering region (CSR) of the initial powder determined for the $MgAl_2O_4$ phase is 38 nm, nanoceramics – 30 nm. Lattice constant of the initial powder a = 8.08344(7) Å, transparent ceramics a = 8.08440(8) Å. The impurity phase of MgO has a spatial group $Fm\bar{3}m$ and a = 4.4124(5) Å for the initial powder and a=4.2126(5) Å for nanoceramics.

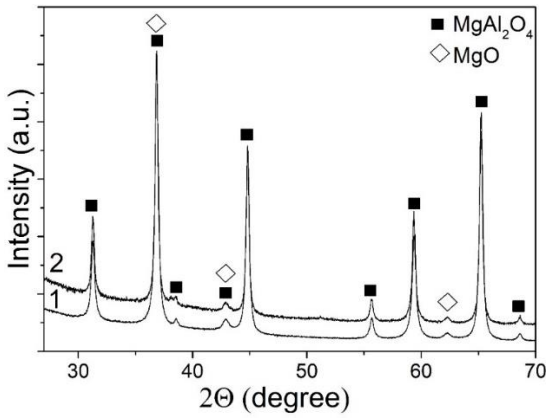

Figure 1. XRD pattern of (1) initial powder and (2) transparent nanoceramics.

3.2. Scanning electron microscopy

SEM images of initial powder (Fig. 2a), as well as nanoceramics (Fig. 2b,c) are presented for different types of magnifications to show the absence of large agglomerates and pores. It is seen from Figure 2a that the initial powder consists of nanograins, agglomerated in large particles. The surface of MAS nanoceramics looks like extended plateaus without large agglomerates. It is important to note that in nanoceramics there are no pores with a diameter of 100 nm or more. Such pores are formed at the boundaries of several grains and are characteristic of microceramics. Another observed feature is the narrow particle size distribution. The distribution of crystallites by size is one of the main parameters that determine the optical and mechanical properties of ceramics. There is also a lack of cracks capable of scattering electromagnetic radiation. Earlier, we showed that they were responsible for transparency [12]. The inset in Figure 2c shows a photograph of the transparent nanoceramics studied.

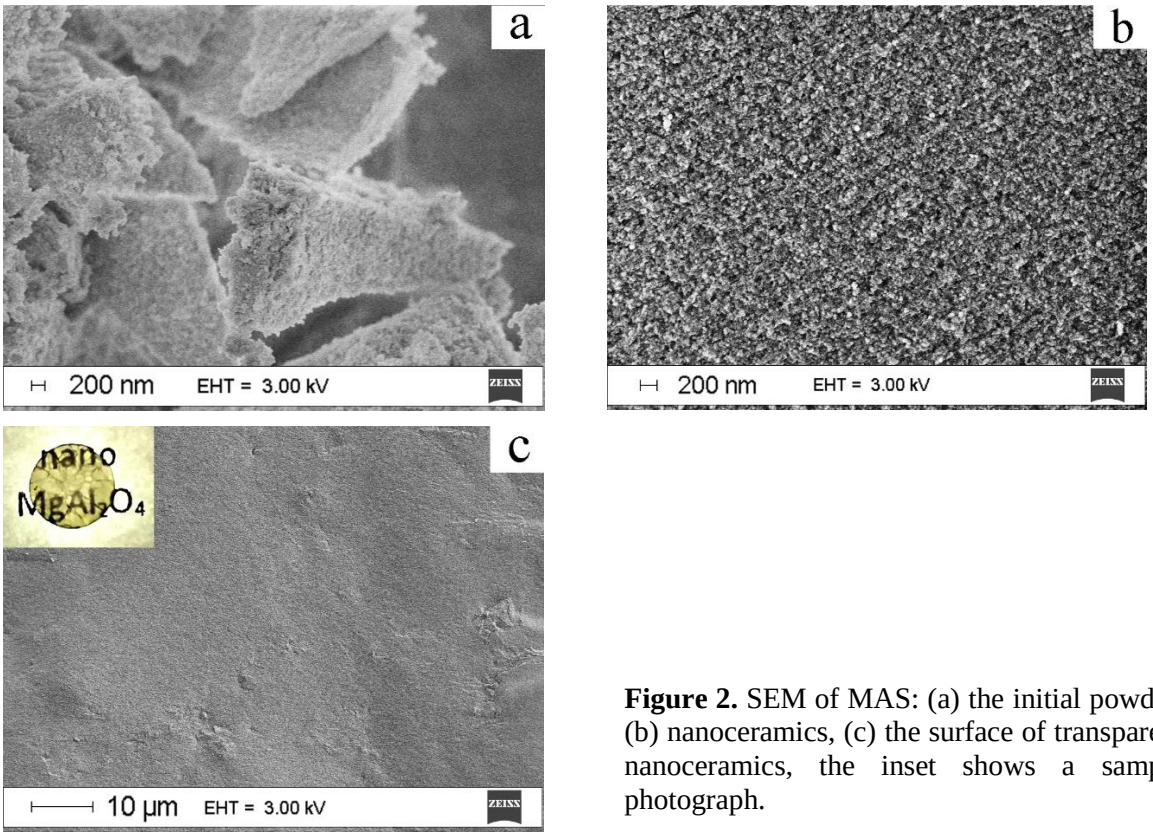

Figure 2. SEM of MAS: (a) the initial powder, (b) nanoceramics, (c) the surface of transparent nanoceramics, the inset shows a sample photograph.

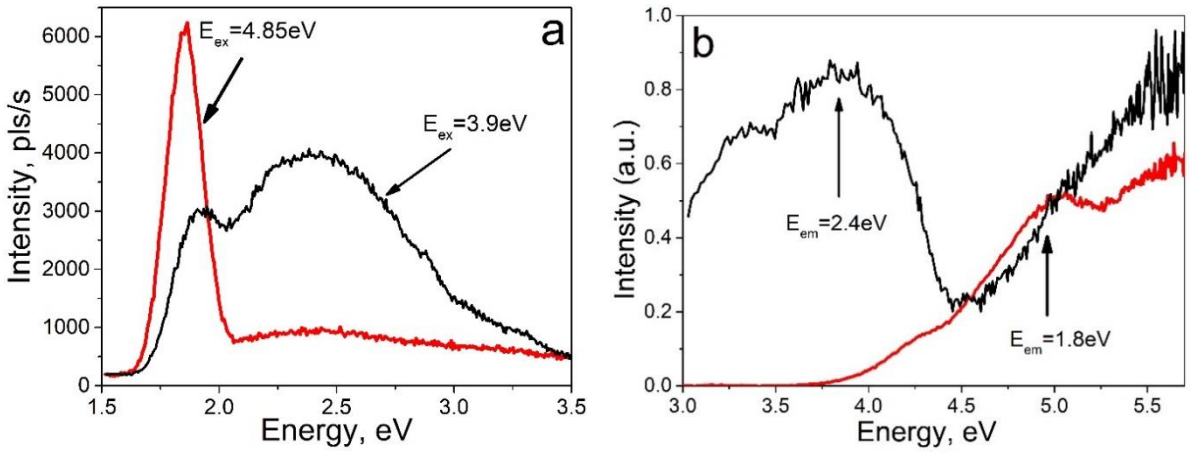

Figure 3. (a) Luminescence and (b) excitation spectra of transparent MAS nanoceramics.

3.3. Photoluminescence

The luminescence and excitation spectra are shown in Figure 3a,b. Two intense bands with maxima at 1.8 and 2.4 eV are observed in the luminescence spectrum. The maximum of excitation band at 1.8 eV is located at 4.85 eV. The 2.4 eV band is most effectively excited at 3.9 eV. It is also worth noting that the luminescent peak at 2.4 eV is greatly broadened. Excitation efficiency of the marked luminescence bands increases when approaching the vacuum UV.

3.4. Electron spin resonance

The ESR spectra are shown in Figure 4a. A wide signal ESR g = 4.39 is observed. In the range of 3000-4000 G there is a series of narrow lines (Fig. 4b). The most intense signals are with g = 2.005 and 1.981. Six narrow, equally spaced lines (A = 90 G) correspond to hyperfine structure.

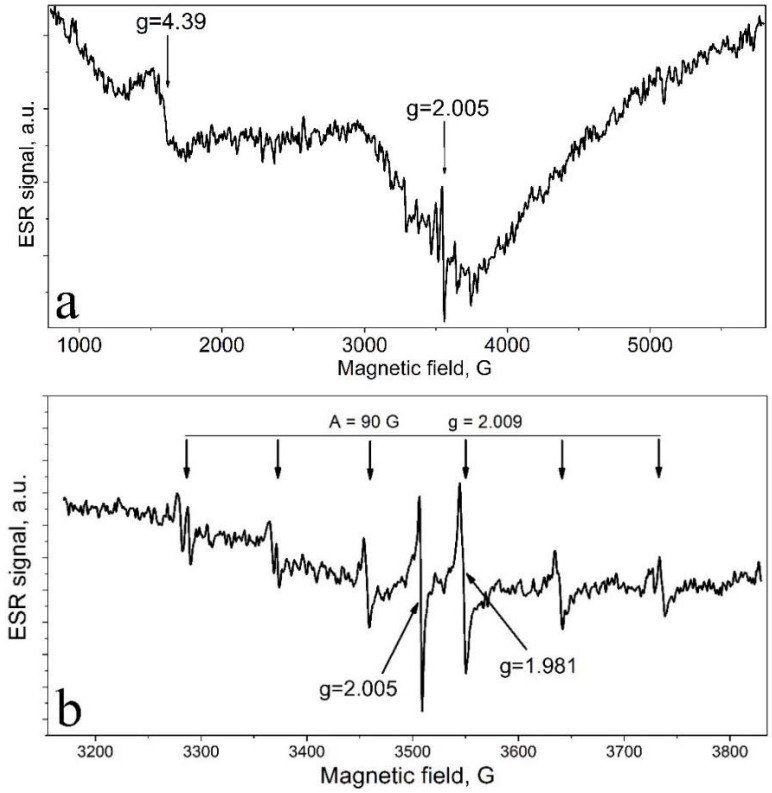

Figure 4. The ESR spectra of nanoceramics MAS.

4. Discussion

Comparing the results of SEM and XRD, we should note the correlation in the recorded particle size (not more than 50 nm). Reduction of CSR in nanoceramics compared to the initial powder is associated with the processes of elastic deformation in the material [7]. The noted growth of the lattice constant for MAS nanoceramics is caused by a large number of substitution defects $[Mg]_{Al}$ and vice versa [13,14].

Thermobaric treatment of the material results in a high degree of compaction, as evidenced by the SEM study. An important characteristic of ceramics is defectiveness. Combining the methods of photoluminescence and EPR allows characterizing the point defects. The luminescence peak at 1.8 eV is due to the presence of trace impurities of octahedral Ti^{3+} in the row materials [15]. The registered excitation band in the UV region is typical for the specified defect. It is worth noting that the maxima positions of the excitation and luminescence bands shift to lower wavelengths region (high energies). The reason for this blue shift is the low grain dimension, which is confirmed by CSR and SEM.

The half-width of 2.4 eV luminescent peak as well as the maximum on the excitation spectrum do not correspond to the literature data. On the one hand, a wide luminescence band with noted maximum can be associated with trace impurities of tetrahedral Mn^{2+} [16]. On the other hand, TBT of $MgAl_2O_4$ could lead to the formation of oxygen vacancies, the luminescence of which in covalent crystals is characterized by significant broadening [17].

ESR spectra make it possible to detect point defects associated with an unpaired electron due to high sensitivity to them. The resonance absorption at g = 4.39 is caused by the trace amount of iron ions in ceramics [18]. According to the characteristic hyperfine structure splitting (hyperfine structure, 6 lines equally spaced from each other), it can be concluded that the nanoceramics contain an uncontrolled impurity of Mn^{2+} ions (g = 2.009). It is known that a narrow signal with g = 2.005 can be associated with oxygen vacancies in MAS [19]. It is worth noting that the 4th line (g = 1.981) of hyperfine structure of manganese ions is much more intense than the others, which may be a consequence of superposition of ESR signals. In the work on the doping of the spinel with titanium ions, the rise of the signal with the specified g-factor is observed [20]. Table 1 contains the main parameters of the registered ESR signals.

Table 1. The main parameters of the ESR signals.

g-factor	4.39	2.009	2.005	1.981
Weight, G	212	8.5	3.8	5.3
Nature	Fe^{3+}	Mn^{2+}	F^{+}-center	Ti^{3+}

Thus, there is a correlation between photoluminescence and ESR spectra. The luminescence in 1.8 eV is due to impurity titanium ions, the broad luminescence band in 2.4 eV is most likely a combination of the luminescence bands of oxygen vacancies and impurity manganese ions in the tetrahedral Mg^{2+} position. These defects are detected by ESR methods using characteristic lines in the spectrum.

5. Conclusion

The transparent nanoceramics of the aluminium magnesium spinel were obtained by thermobaric treatment in a toroidal chamber. It was established that the main phase of the nanoceramics obtained was $MgAl_2O_4$ with an insignificant fraction of MgO (~3%). The structural features of the resulting transparent nanoceramics are: absence of cracks, narrow grain size distribution, cationic inversion with formation $[Mg]_{Al}$ defects, and vice versa. An important feature of the obtained ceramics is the absence of large pores, which reduce the transparency.

The presence of Ti^{3+} and Mn^{2+} impurity centres was determined by the characteristic bands using luminescence and ESR methods. A blue shift of the emission band of Ti^{3+} ions is associated with the size effect. An abnormally wide 2.4 eV emission band is presumably associated with the luminescence of Mn^{2+} combined with luminescence of oxygen vacancies (F and F^{+} centres).

Acknowledgments
The work was done as a part of the government task (№3.1485.2017/4.6) of the Ministry of Education and Science of the Russian Federation and was carried out in accordance with the scientific and research plans and state assignment of the Institute of Solid State Chemistry of the Ural Branch of the Russian Academy of Sciences (AAAA-A16-116122810212-5).

References
[1] Sai Q, Xia C, Rao H, Xu X, Zhou G and Xu P 2011 *J. Luminescence* **131** 2359-64
[2] Aizawa H, Ohishi N, Ogawa S, Watanabe E, Katsumata T, Komuro S, Morikawa T and Toba E 2002 *Rev. Sci. Instr.* **73** 3089-92
[3] Sanghera J, Bayya S, Villalobos G, Kim W, Frantz J, Shaw B, Sadowski B, Miklos R, Baker C, Hunt M, Aggarwal I, Kung F, Reicher D, Peplinski S, Ogloza Al, Langston P, Lamar C, Varmette P, Dubinskiy M and DeSandre L 2011 *Opt. Mat.* **33** 511-8
[4] Clinard Jr F W 1987 *Cer. Int.* **13** 69-75
[5] Rubat du Merac M, Kleebe H J, Müller M M and Reimanis I E 2013 *J. Am. Cer. Soc.* **96** 3341-65
[6] Bergmann C P and Stumpf A 2017 *Topics in mining, metallurgy and materials engineering* Porto Alegre: Springer.
[7] Zou Y, He D, Wei X, Yu R, Lu T, Chang X, Wang Sh and Lei L 2010 *Mat. Chem. Phys.* **123** 529
[8] Lu T C, Chang X H, Qi J Q, Luo X J, Wei Q M, Zhu S, Sun K, Lian J and Wang L M 2006 *Appl. Phys. Lett.* **88** 213120
[9] Vahid B R and Haghighi M 2017 *Energy Convers. Manag.* **134** 290-300
[10] Toby B H 2001 *J. Appl. Cryst.* **34** 210-3
[11] Larson A C and Von Dreele R B 1994 *Report LAUR* 86-748
[12] Kiryakov A N, Zatsepin A F, Slesarev A I, Dyachkova T V, Zainulin Yu G, Mashkovtsev M, Yakovlev G and Vagapov A Sh 2018 *AIP:Conf. Proc.* **2015** 020039
[13] Méducin F, Redfern S A, Le Godec Y, Stone H J, Tucker M G, Dove M T and Marshall W G 2004 *Am. Mineralogist* **89** 981-6
[14] Ball J A, Pirzada M, Grimes R W, Zacate M O, Price D W and Uberuaga B P 2005 *J. Phys.: Cond. Matt.* **17** 7621-31
[15] Sato T, Shirai M, Tanaka K, Kawabe Y and Hanamura E 2005 *J. Luminescence* **114** 155-61
[16] Singh V, Chakradhar R P S, Rao J L and Kim D K 2007 *J. Solid State Chem.* **180** 2067-74
[17] Sawai S and Uchino T 2012 *J. Appl. Phys.* **112** 103523
[18] Cannas C, Gatteschi D, Musinu A, Piccaluga G and Sangregorio C 1998 *J. Phys. Chem. B* **102** 7721-6
[19] Ibarra A, Bravo D, Lopez F J and Garner F A 2005 *J. Nucl. Mater.* **336** 156-62
[20] Lombard P, Boizot B, Ollier N, Jouini A and Yoshikawa A 2009 *J. Cryst. Growth* **311** 899-903